Phase transitions and topological properties of the $\frac{5}{2}$ quantum Hall states with strong Landau-level mixing

Wenchen Luo,[1] Wei Zhang,[1] Yutao Hu,[1] and Hao Wang[2,3,4,*]

[1]*School of Physics and Electronics, Central South University, Changsha 410083, China*

[2]*Shenzhen Institute for Quantum Science and Engineering, Southern University of Science and Technology, Shenzhen 518055, China*

[3]*International Quantum Academy, Shenzhen 518048, China*

[4]*Guangdong Provincial Key Laboratory of Quantum Science and Engineering, Southern University of Science and Technology, Shenzhen 518055, China*

(Received 30 October 2022; revised 12 December 2022; accepted 19 December 2022; published 26 December 2022)

We numerically study a $\frac{5}{2}$ fractional quantum Hall system with even number of electrons using the exact diagonalization where both the strong Landau-level (LL) mixing and a finite width of the quantum well have been considered and adapted into a screened Coulomb interaction. With the principal component analysis, we are able to recognize a compressible-incompressible phase transition in the parameter space made of the magnetic field and the quantum well width by the competition between the first two leading components of the ground-state wave functions, which is consistent with the low-lying spectral feature and previous works in the odd-electron system. In addition, the presence of the subdominant third component suggests an incompressible transition occurring as the LL mixing strength grows into a certain parameter region associated with the ZnO experiments. We further investigate the strongly LL-mixed phase in this emerging region with the Hall viscosity, wave function overlaps, and the entanglement spectra. Results show it can be well described as a particle-hole symmetrized Pfaffian state with the dual topological properties of the Pfaffian and the anti-Pfaffian states.

DOI: 10.1103/PhysRevB.106.245142

I. INTRODUCTION

The nature of the even denominator fractional quantum Hall effect (FQHE) is still unclear in many aspects [1]. In wide or double quantum wells, even denominator FQHE can be explained by the Halperin state [2]. But for those FQHEs with non-Abelian excitations, an understanding for their nature is still a puzzle. For $\frac{5}{2}$ FQHE, the Pfaffian [3] or anti-Pfaffian wave function [4] is proposed to be the most promised candidate. However, either the numerical calculation of wave function overlaps or the thermal conductance experiment [5] challenges these trial wave functions. Some theoretical approaches try to explain the thermal conductance experiment by modeling the ground state with Pfaffian–anti-Pfaffian domains [6] or by considering the partial equilibration of the thermal transport [7]. Other trial wave functions are also proposed in the spirit of the composite fermion paring [8,9]. However, they are either energetically unfavorable or unmatched with numerical overlap calculations. Nevertheless, the topologically nontrivial feature of the $\frac{5}{2}$ FQHE, which is experimentally confirmed by the Majorana mode with $\frac{1}{2}$ thermal Hall conductance, should be recognized.

In studying the FQHE of a realistic two-dimensional electron gas (2DEG), Landau level (LL) mixing is an important effect to be considered. To scale the strength of the LL mixing, one must define a dimensionless parameter $\kappa = E_C/E_{LL}$ where $E_C = e^2/\epsilon\ell$ is the Coulomb interaction strength and $E_{LL} = \hbar\omega_c$ is the LL gap with the cyclotron frequency $\omega_c = |e|B/m^*$ where e is the electron charge, B the magnetic field, and m^* the effective mass. If $\kappa \to 0$, the LLs are considered infinitely gapped and thus the LL mixing is negligible.

For the GaAs quantum well, considering the material parameters and the magnetic field used in experiments, the LL mixing there has a moderate strength with $\kappa \sim 1$, which is strong enough to affect the nature of the FQHE state. It has been argued that the perturbative theory would still be feasible and the induced three-body interaction will break the particle-hole (PH) symmetry [10]. Given that the (anti)Pfaffian state is the unique zero-energy state of some three-body interaction in a half-filled system, the $\frac{5}{2}$ FQHE state is thus related to a Pfaffian or an anti-Pfaffian state when the LL mixing is taken into account. However, in the ZnO/MgZnO heterostructure [11–13] or black phosphorene [14] the effective mass of the electron is about one magnitude higher than that in a GaAs quantum well, leading to an extremely large $\kappa \gg 1$. There, the LL mixing is so strong that the perturbative theory could not be available. More importantly, the strong LL mixing has been argued possible to recover the particle-hole symmetry [15], which will be reclaimed in this work. It is reasonable to expect that the ground states of the $\frac{5}{2}$ FQHEs in the ZnO quantum well should be biased from that in GaAs.

For a strongly LL mixing system with a finite filling (for instance, $\nu = \frac{5}{2}$), the electrons are distributed in far more than three LLs, causing a huge Hilbert space. The computer resource for such a large system would be exhausted in most conventional approaches. A substitutive way to study the strongly LL-mixed system is to project the 2DEG into a single

*wangh@sustech.edu.cn

relevant LL with the effectively screened Coulomb interaction in the random-phase approximation (RPA) [16–18], of which the Hilbert space is sufficiently small for the exact diagonalization scheme. The screened Coulomb potential containing the information of all the other LLs can be used to interpret the stability of the $\frac{5}{2}$ FQHE [17,19], which agrees with the experimental results [11,12]. In our present work on the strongly LL-mixed $\frac{5}{2}$ fractional quantum Hall system with a finite width of the quantum well, we adopt the same screening treatment for the electron-electron interaction to construct an effective model Hamiltonian. With the numerical spectra and principal component analysis (PCA) [20] on the ground-state wave functions, we obtain a phase diagram in the parameter space consisting of the magnetic field and the width of the quantum well with several phase transitions. An incompressible phase with a large LL mixing strength can be associated to parameters of the ZnO samples, and physical properties of its ground state are investigated through the calculations of the Hall viscosity, wave function overlaps, and the entanglement spectra [21].

II. MODEL HAMILTONIAN

We consider a $\frac{5}{2}$-filling FQHE system with the 2DEG extended a bit in the perpendicular (z) direction due to the finite width of the quantum well. For simplicity, the confinement potential of the quantum well is assumed to be an infinity square well. Thus, the z component of the wave function is given by $\phi_m(z) = \sqrt{2/L_z}\sin(m\pi z/L_z)$ with the quantum number m indexing the band and L_z for the width of the quantum well. The full wave function of the 2DEG takes a two-part form as $\Psi(\mathbf{r}, z) = \phi_m(z)\psi(\mathbf{r})$, where $\mathbf{r}$ is the in-plane coordinate. On the torus, the in-plane part of the wave function has the form of $\psi_{n,i}(\mathbf{r})$ in the Landau gauge with n for the LL index and i for the guiding center index. On a sphere, the in-plane part ψ should be replaced by the wave function on the zero-width sphere, and i for the angular momentum.

In the toroidal geometry, the many-body Hamiltonian of a Coulomb interaction system is given by

$$H = \sum_{n,i,\sigma} E_{n,\sigma} c^\dagger_{n,i,\sigma} c_{n,i,\sigma} + \frac{1}{2}\sum_{\sigma,\sigma'}\sum_{\substack{n_1,\ldots,n_4\\ i_1,\ldots,i_4}} V^{n_1,n_2,n_3,n_4}_{(s),i_1,i_2,i_3,i_4} \times c^\dagger_{n_1,i_1,\sigma} c^\dagger_{n_2,i_2,\sigma'} c_{n_3,i_3,\sigma'} c_{n_4,i_4,\sigma}, \tag{1}$$

where the first term is kinetic energy with the summation over all LL indices n, guiding center indices i, and spin indices σ. Symbol c ($c^\dagger$) stands for electron annihilation (creation) operator. As to the electron-electron interaction term, considering the strong LL mixing, we treat it with the screening scheme as modeled in Ref. [19]. The electron distribution is the same as the noninteracting picture so that we can concentrate ourselves on the highest occupied LL, in which the electron-electron interaction is screened by all the virtual processes between the LLs with different filling in the RPA. We believe that this screening scenario is a good approach to describe the strongly LL-mixed system although some of the correlations are neglected. Under such treatment, we can constrain the system in the half-filled $n = 1$ LL. If all electrons can be regarded fully spin polarized due to the large magnetic field [17], the Hamiltonian is reduced to

$$H = \frac{1}{2}\sum_{i_1,\ldots,i_4} V^{n,s}_{i_1,i_2,i_3,i_4} c^\dagger_{i_1} c^\dagger_{i_2} c_{i_3} c_{i_4}, \tag{2}$$

where the screened Coulomb interaction matrix element has the form of

$$V^{n,s}_{i_1,i_2,i_3,i_4} = \frac{e^2}{\epsilon\ell}\frac{2}{\pi N_s}\overline{\sum_{\mathbf{q}}}\delta'_{i_1,i_4+q_y\ell^2}\delta'_{i_2,i_3-q_y\ell^2} e^{iq_x\ell^2(i_3-i_1)} \times e^{-q^2\ell^2/2}\left[L_n\left(\frac{q^2\ell^2}{2}\right)\right]^2 V_s(q). \tag{3}$$

In the above expression, $\mathbf{q}$ is the discrete in-plane momentum, N_s is the LL degeneracy, δ' includes the periodic boundary condition, $L_n(x)$ is a Laguerre polynomial, and $\overline{\sum}$ means that the $q = 0$ term is excluded in the summation.

As we consider only the first band at $m = 1$, the effective Coulomb potential $V_s(q)$ is given by

$$V_s(q) = \int_0^\infty \frac{32\pi^4 dq_z\ell}{\epsilon_s(q,q_z)\left(q^2+q_z^2\right)\ell^2}\frac{1-\cos(q_zL_z)}{\left(4\pi^2 q_zL_z - q_z^3L_z^3\right)^2}. \tag{4}$$

Such dressed Coulomb potential is obtained by the pure Coulomb potential divided by the static dielectric function $\epsilon_s(q, q_z)$. In calculating the dielectric function, we use the noninteracting retarded density-density response function $\chi^0_{nn}(q, q_z, \omega \to 0)$ in the RPA in the static limit for simplicity. The dielectric function is then given by

$$\epsilon_s(q,q_z) = 1 - \frac{4\pi e^2}{\left(q^2+q_z^2\right)\epsilon}\chi^0_{nn}(q,q_z) \tag{5}$$

with

$$\chi^0_{nn}(q,q_z) = \chi^0_{nn}(q,q_z,\omega\to 0) = \frac{1}{2\pi\ell^2 L_z}\sum_\sigma\sum_{m_1,n_1}\sum_{m_2,n_2}\left|G^{m_1,n_1}_{m_2,n_2}(\mathbf{q},q_z)\right|^2 \times \frac{\nu_{(m_1,n_1),\sigma} - \nu_{(m_2,n_2),\sigma}}{E_{(m_1,n_1),\sigma} - E_{(m_2,n_2),\sigma}}, \tag{6}$$

where m_i and n_i mark the band and the LL indices, and $E_{(m_1,n_1),\sigma}$ and $\nu_{(m_1,n_1),\sigma}$ are the kinetic energy and the filling factor of the LL (m_1, n_1) with spin σ, respectively. The form factor is written as $G^{m_1,n_1}_{m_2,n_2}(\mathbf{q}, q_z) = iq_zL_zF_{n_1,n_2}(-\mathbf{q})g_{m_1,m_2}(-q_z)$ with the functions

$$F_{n,n'}(\mathbf{q}) = \frac{\sqrt{\min(n,n')!}}{\sqrt{\max(n,n')!}}e^{-q^2\ell^2/4}L^{|n-n'|}_{\min(n,n')}\left(\frac{q^2\ell^2}{2}\right) \times \left[\frac{\mathrm{sgn}(n-n')q_y\ell + iq_x\ell}{\sqrt{2}}\right]^{|n-n'|}, \tag{7}$$

$$g_{m_1,m_2}(q_z) = [1 - e^{iq_zL_z}\cos(m_1-m_2)\pi] \times \left[\frac{1}{(m_1-m_2)^2\pi^2 - q_z^2L_z^2} - \frac{1}{(m_1+m_2)^2\pi^2 - q_z^2L_z^2}\right]. \tag{8}$$

The expression of Eq. (6) indicates a summation over all LLs. In practice, it is necessary to set a truncation since the high-energy LLs contribute little to the studied system.

In the spherical geometry, the Hamiltonian can also be written in a form similar to Eq. (2) by using Haldane's pseudopotential

$$V_i^s = \int_0^\infty \frac{dq^2\ell^2}{\pi}\left[L_n\left(\frac{q^2\ell^2}{2}\right)\right]^2 e^{-q^2\ell^2} L_i(q^2\ell^2)V_s(q), \quad (9)$$

where we approximately use the planar pseudopotential and both the thickness and the screening corrections have been included in $V_s(q)$.

As shown in the above effective Hamiltonians, both the strength of the magnetic field and the width of the quantum well will soften the Coulomb interaction and thus significantly modify the properties of the strongly correlated system. Topological phase transitions might occur [18] given continuous variations in the parameter space made of B and W, which is the half-width of the wave function in the z direction and $W = L_z/1.5$ for an infinity square well. Such possible phase transitions and the topological features of the corresponding quantum states can be explored through the calculated energy spectra and state wave functions as we numerically solve the model Hamiltonians using the exact diagonalization. Since different topological states on the sphere may correspond to different spherical shifts, thus different Hilbert spaces, it could be difficult to probe a possible topological phase transition with continuously varying parameters in the spherical geometry. Therefore, in our analysis we mainly take the toroidal geometry [22,23]. The parallelogram unit cell of the torus is framed by two basis vectors $\vec{L}_1$ and $\vec{L}_2$ with the aspect ratio $|\tau| = L_1/L_2$ and the aspect angle θ between them. Within the cell, there are N_e electrons and N_s magnetic flux quanta with $N_s = 2N_e$ corresponding to the half-filled second LL. Several state wave functions in the spherical geometry at specified spherical shifts are also studied for comparison purposes.

III. PHASE TRANSITIONS

In a previous work [19], strongly LL-mixed systems with odd number of electrons on the torus have been studied in the (B, W) parameter space. The compressible-incompressible phase transition is detected there by monitoring the variation of the excitation energy gap. The 2DEG is found generally incompressible in the $BW > 30$ T nm region and the phase diagram can be used to explain the missing or the appearance of the experimental observation of the $\frac{5}{2}$ FQHE in different ZnO samples [12,13]. However, considering the underlying pairing nature of the even denominator FQHE, a study on an even-electron system would be more relevant and may provide more fundamental information. Different from an odd-electron system where the ground state is nondegenerate and a well-defined excitation gap can serve as the incompressibility probe, an even-electron system on the torus can have its ground state locating "degenerately" at three characteristic pseudomomentum sectors $(N_e/2, 0)$, $(0, N_e/2)$, and $(N_e/2, N_e/2)$ (with the twofold center-of-mass degeneracy subtracted) due to the topological nature of the Pfaffian state [24] and the complete degeneracy is lifted in a finite-sized system. Thus, for the even-electron system in our consideration it is in doubt whether we still can determine an incompressible gap to detect the phase transition. Nevertheless, we can first observe the low-lying energy spectra of the system at distinct phase regions to gain a general impression.

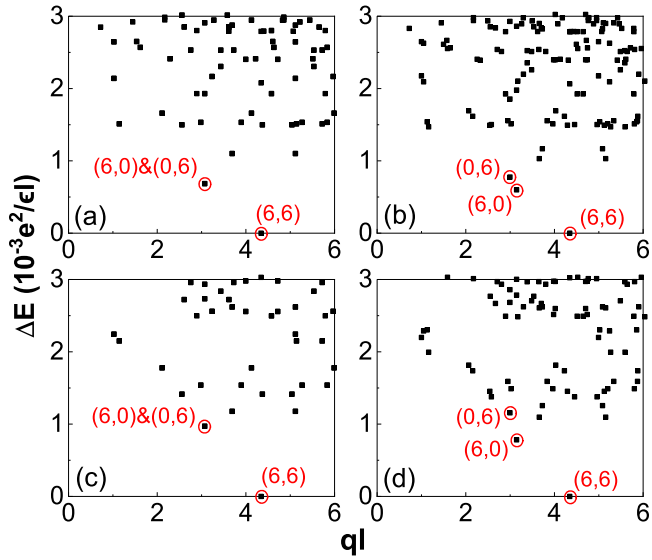

FIG. 1. The low-lying excitation spectra of an $N_e = 12$ system on the torus with a square unit cell for (a) and (c) but a rectangular cell of the aspect ratio $|\tau| = 0.95$ for (b) and (d). The parameter set ($B = 9.6$ T, $W = 5$ nm) used in (a) and (b) stands for the experimental ZnO sample a while ($B = 7.2$ T, $W = 5$ nm) in (c) and (d) for sample b. The ground states at three characteristic pseudomomentum sectors have been labeled and marked in the spectra.

A. Energy spectra

To get a close comparison with the experimental results of the ZnO quantum well [12], we investigate the excitation spectra of the even-electron systems at two selected parameter sets. One is corresponding to the incompressible 2DEG in the sample a ($B = 9.6$ T and $W = 5$ nm) and the other ($B = 7.2$ T and $W = 5$ nm) for the compressible 2DEG in sample b. The material parameters are adopted from the ZnO for the effective mass $m^* = 0.3m_e$ with electron mass m_e and the dielectric constant $\epsilon = 8.5$.

In Fig. 1, we show the low-lying spectra of an $N_e = 12$ system with a square unit cell and a more general rectangular cell at $|\tau| = 0.95$. The systems with less electrons exhibit similar spectra. As seen in Figs. 1(a) and 1(b) for the incompressible sample a, the lowest three states remain staying at the three characteristic sectors of (0,6), (6,0), and (6,6), alike the Pfaffian state on the torus. If we treat them collectively as a threefold manifold gapped from other higher energy states, we note this separation gap and the splitting band width among them are sensitive to the cell geometry. For instance, the three states would be degenerate with a hexagonal cell. However, for the compressible sample b, this general feature of characteristic threefold manifold is missing though the (6,6) state remains as the global ground state. In Fig. 1(c), the lowest (0,6) state and the lowest (6,0) state (degenerate pair due to the additional symmetry of the square cell) are much closer to the upper states in comparing with the incompressible sample

case. In Fig. 1(d) with a rectangular cell, the lowest (0,6) state is lifted from the lowest (6,0) state and no longer holds in the characteristic threefold manifold since some states at other sectors have lower energies.

These spectral observations suggest the incompressible phase can be qualitatively associated with the form of the characteristic threefold manifold. However, due to the finite-size effect it is ambiguous to define an energy gap between this manifold and a higher excitation level. Moreover, this manifold is only valid for the ground state with Pfaffian-like properties. These issues limit our ability of using the energy spectrum alone to quantitatively detect the compressible-incompressible transition for an even-electron system. Instead, we use calculated wave functions as the probe for the phase transition. Considering the lack of explicit knowledge for the quantum states at different phase regions, we exploit the PCA method to analyze the system as described in the next section.

B. Principal component analysis

As an unsupervised machine learning approach, PCA has been applied to study quantum phases in several FQHE systems [20]. There, distinct principal components (PCs) are extracted directly from the parametrized wave functions using a singular value decomposition technique. By tracing the evolution and switching of the predominant PCs, one is able to categorize different quantum phases and detect their transitions.

In our PCA practice, considering the spectral features and the importance of the three lowest states in the characteristic sectors $(N_e/2, 0)$, $(0, N_e/2)$, and $(N_e/2, N_e/2)$, the input data are taken from the ground-state wave functions at these characteristic sectors and the investigated parameter space spans in a range of $B \in [1, 20\ \mathrm{T}]$ and $W \in [1, 16\ \mathrm{nm}]$ in adapting to the ZnO experiments. For simplicity, we consider the LL-mixed system with a square unit cell and an even number of electrons up to $N_e = 12$. Since the $(N_e/2, 0)$ state and the $(0, N_e/2)$ state are degenerate due to the square symmetry, we discuss only the $(0, N_e/2)$ and $(N_e/2, N_e/2)$ states in the following. By monitoring the weights of PCs in the considered parameter space, we note only a few PCs [two for the $(0, N_e/2)$ state and three for the $(N_e/2, N_e/2)$ state] exhibit significant nonzero presence with their sum weight near unity and other PCs are negligible. Therefore, we focus on these leading PCs in our analysis. By tracing the relative evolution of the leading PCs, we are able to draw a phase diagram of an example $N_e = 12$ system as shown in Fig. 2.

For the lowest (0,6) state, there are two leading PCs competing and their weights switch along a curved boundary (dashed purple line) in the parameter space as shown in Fig. 2(a), indicating the occurrence of a phase transition. We note that an earlier work [19] with an odd-electron ($N_e = 11$) system has obtained a similar phase diagram where the compressible and incompressible phase regions are identified through the incompressible gap. Mapping with those results, we expect the parameter region in our diagram with the large B and W, i.e., the first PC-dominated region, would correspond to an incompressible phase while the phase at the opposite side would be compressible. The further evidences are shown

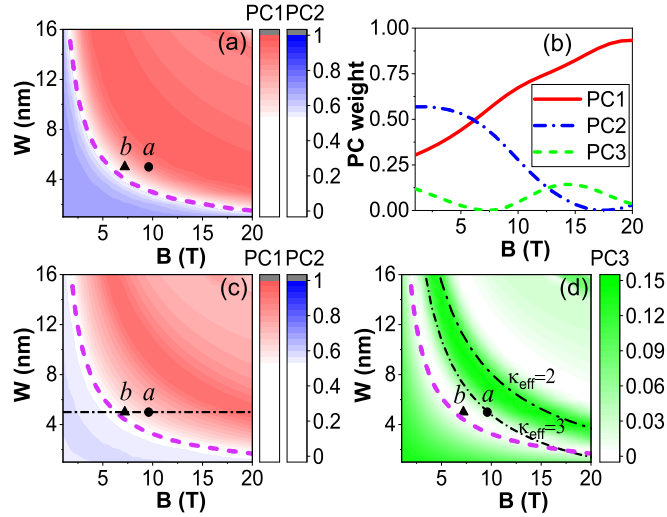

FIG. 2. Weight distributions of the leading PCs in the (B, W) parameter space for the manifold states of an $N_e = 12$ system on the torus with a square unit cell. The plot (a) stands for two leading PCs of the ground state at the (0,6) pseudomomentum sector where the dashed (purple) curve sketches the compressible-incompressible phase boundary by the switching of the two PCs and the locations of the experimental ZnO samples a and b are marked. The plot (b) shows the weights of three leading PCs as a function of B for the ground state at the (6,6) sector when the width is fixed to $W = 5$ nm. The plot (c) stands for the first two PCs of the (6,6) ground state with the dot-dashed line corresponding to the plot (b). The plot (d) stands for the third leading PC of the (6,6) ground state with its largest distribution inside the incompressible region mostly falling in the range of $\kappa_{\mathrm{eff}} \in [2, 3]$.

as we mark two experimental samples with their corresponding parameters in the diagram. Although both samples seem to be locating in the assumed incompressible side, the sample b is already much closer to the boundary. One might suspect the sample b, that actually falls in the transition zone, to be more compressible especially at finite temperature, which is also demonstrated by its low-lying spectra.

For the (6,6) ground state, there exist three leading PCs; one example is shown in Fig. 2(b) for the wave functions at the width $W = 5$ nm. The competition and switching between the first two PCs provide us with a similar phase diagram for the compressible-incompressible phase transition as shown in Fig. 2(c) while the subdominant third PC presents some extra feature. Within the incompressible zone, we note that there is a narrow region near the compressible-incompressible phase boundary where the third PC emerges accompanied with the suppression of the second PC. If we define a rescaled LL mixing parameter $\kappa_{\mathrm{eff}} = e^{-L_z/\ell} E_C/E_{LL}$ in considering the effect of the finite width of the quantum well, this particular region mostly locates within the range of $\kappa_{\mathrm{eff}} \in [2, 3]$ as shown in Fig. 2(d). Since the composition of the PCs at this region is different from that with less κ_{eff}, a phase transition is suspected as the LL mixing strength of an incompressible system grows to the $\kappa_{\mathrm{eff}} \in [2, 3]$ range. We note some earlier experimental and numerical work [18,25] for a strong LL-mixed system with zero-width quantum well have suggested a possible phase transition occurring within

the incompressible range $\kappa \in [2, 3]$. Our discovery with the subdominant PC supports their results.

IV. INCOMPRESSIBLE QUANTUM STATE WITH STRONG LL MIXING

For the incompressible phase at small LL mixing, a few of the earlier theoretical and numerical works have proposed it to be a Pfaffian or an anti-Pfaffian state due to perturbative three-body interactions. At large LL mixing where the perturbation theory is invalid, our treatment in previous sections with a screened Coulomb interaction suggests an incompressible phase transition emerges as the growing LL mixing strength approaches the $\kappa_{\text{eff}} \in [2, 3]$ range. Even if we leave the incompressible region with less κ_{eff} as a transition zone from the small perturbative LL mixing phase, there is an absence of knowledge for the incompressible states within the emerged phase region $\kappa_{\text{eff}} \in [2, 3]$. In this section, we will investigate the physical properties of the quantum states in this region. Note that the incompressible sample a of the ZnO experiment [12] locates within this region, and in the following discussion we choose the corresponding parameter set ($B = 9.6$ T and $W = 5$ nm) as the representative case for a better understanding of the experiments.

A. Hall viscosity

Hall viscosity, which is defined as $\eta = \frac{1}{2}\bar{s}\bar{n}\hbar$ with the average particle density $\bar{n}$ and the average orbital spin per particle $\bar{s}$, has been used to characterize the topological property of a FQHE state [26]. It is closely related to the spherical shift S, which is another topological probe defined on the sphere [27], by relation of $S = 2\bar{s}$. On the torus, given the geometry is parametrized by a complex number $\tau = \tau_1 + i\tau_2 = |\tau|e^{i\theta}$, the mean orbital spin $\bar{s}$ (as well as the relevant η and S) can be calculated through the Berry phase of a considered many-body state Ψ when it adiabatically varies around an enclosed path in the geometric parameter space. For a circular path around a center τ_0 and with a radius $\rho_0 (< \tau_{20})$, it gives

$$\bar{s} = \frac{1}{2} + \frac{1}{2\pi}\text{Im}\iint d\tau_1 d\tau_2 \left\langle \frac{\partial\Psi}{\partial\tau_1} \middle| \frac{\partial\Psi}{\partial\tau_2} \right\rangle \Big/ D, \qquad (10)$$

with the normalization factor $D = N_e[\frac{1}{\sqrt{1-(\rho_0/\tau_{20})^2}} - 1]$. In our numerical study, the integral in the second term of Eq. (10) is evaluated by evenly discretizing the circular path into M pieces and the result then can be counted as a sum of the normalized local Berry curvature as $\sum_{k=1}^{M} B_k$. The topological nature of an incompressible state requires the calculated orbital spin $\bar{s}$ (or shift S) to converge to a certain rational number for a small ρ_0 and a large M, regardless of the choice of τ_0, e.g., $\bar{s} = \frac{3}{2}$ for Pfaffian state and $\bar{s} = -\frac{1}{2}$ for anti-Pfaffian state.

We take Hall viscosity as our first probe of the topological property of the incompressible state with strong LL mixing. For a system associated with the representative parameter set, we focus on the three lowest states in the characteristic threefold manifold. The mean orbital spin of the ground state at each characteristic pseudomomentum sector is calculated and the results for an example $N_e = 12$ system with $M = 200$ and $\rho_0 = 0.001$ are shown in Fig. 3. Other smaller systems are found owning quantitatively similar features.

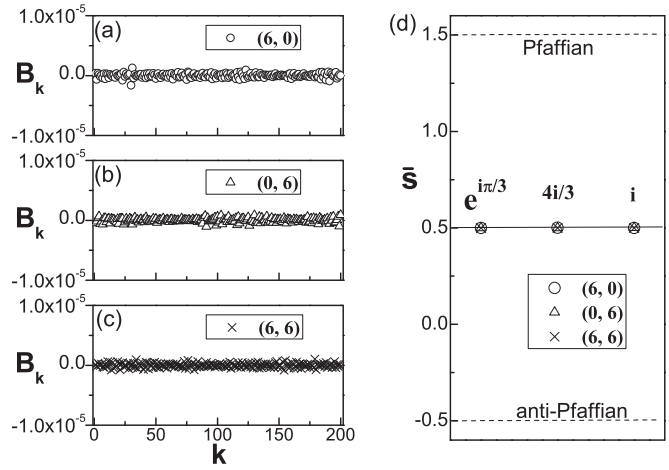

FIG. 3. The local Berry curvature for the ground states of the $N_e = 12$ Coulomb system at pseudomomenta (a) (6,0), (b) (0,6), and (c) (6,6). In the calculation we used 200 discrete steps along a circular path with its center $\tau_0 = i$ (square geometry) and radius $\rho_0 = 0.001$. The resultant $\bar{s}$ around different circular paths are collected in (d) where their corresponding centers τ_0 are labeled and two dashed lines mark the expected values for a Pfaffian state and an anti-Pfaffian state as a comparison.

As presented in Figs. 3(a)–3(c), the local Berry curvatures are homogeneously close to zero in the whole integral region, resulting in a vanished sum for the Berry phase. The smooth distribution of the local Berry curvature without dramatic fluctuations indicates that the investigated state carries a stable topological order. Furthermore, the consequent $\bar{s}$ are plotted in Fig. 3(d) for different integral paths, indicating a universal convergence to $\bar{s} = 1/2$, which is neither the expected value for the Pfaffian state nor for the anti-Pfaffian state. Note that a particle-hole symmetric state at half-filling has $\bar{s} = \frac{1}{2}$; our numerical results suggest the investigated incompressible state would more likely be a PH symmetric state rather than a PH-asymmetric Pfaffian or anti-Pfaffian state. One would not be surprised by the PH symmetry of the ground state as confirmed by the above calculation since the screened Coulomb potential is essentially a two-body interaction. At strong LL mixing, we believe this RPA renormalized two-body interaction is sufficient enough to make the system regain the PH symmetry which could be broken in the appearance of perturbative three-body interactions in less LL mixing cases.

B. Wave function overlap

Considering the alike spectral feature with the same characteristic threefold manifold as the Pfaffian ($|pf\rangle$) or anti-Pfaffian ($|apf\rangle$) state and the PH-symmetric nature revealed through the Hall viscosity calculation, it is reasonable to construct a PH-symmetrized Pfaffian state ($|spf\rangle$) as a possible candidate state to describe the incompressible system at large LL mixing. Such symmetrized state is an equal weight superposition of a Pfaffian state and its particle-hole

TABLE I. The wave function overlaps between the Coulomb ground states at three characteristic pseudomomentum sectors and the candidate model states of the Pfaffian $|pf\rangle$, anti-Pfaffian $|apf\rangle$, and PH-symmetrized Pfaffian $|spf\rangle$ for an $N_e = 12$ system on the torus with a square unit cell at the parameter set ($B = 9.6$ T, $W = 5$ nm).

	$\lvert\langle pf\lvert\text{GS}\rangle\rvert$	$\lvert\langle apf\lvert\text{GS}\rangle\rvert$	$\lvert\langle spf\lvert\text{GS}\rangle\rvert$
$(\frac{N_e}{2}, 0), N_e = 10$	0.797	0.797	0.973
$(0, \frac{N_e}{2}), N_e = 10$	0.797	0.797	0.973
$(\frac{N_e}{2}, \frac{N_e}{2}), N_e = 10$	0.73	0.73	0.989
$(\frac{N_e}{2}, 0), N_e = 12$	0.76	0.76	0.958
$(0, \frac{N_e}{2}), N_e = 12$	0.76	0.76	0.958
$(\frac{N_e}{2}, \frac{N_e}{2}), N_e = 12$	0.776	0.776	0.949

flipped state ($\overline{|pf\rangle}$) in a non-normalized form of $|spf\rangle = |pf\rangle \pm \overline{|pf\rangle}$. For a $\frac{5}{2}$ FQHE system with neglected LL mixing effect, numerical studies showed $|spf\rangle$ can have a much larger overlap with the system ground state when comparing with the (anti-)Pfaffian state. For the strong LL mixing system, we carry out the same exam with the wave function overlap. The (anti-)Pfaffian states used in the calculation are generated as the densest zero-energy ground state of a three-body pseudopotential [28,29].

In Table I, we list the numerical results for a representative system with the square unit cell but different electron numbers. The ground states ($|\text{GS}\rangle$) of the screened Coulomb potential at three characteristic sectors are all investigated. The system ground state has exactly equal overlap with a Pfaffian state and with an anti-Pfaffian state but the value is no more than 0.80. Contrarily, the wave function overlap between the Coulomb ground state and the PH-symmetrized state is generally larger than 0.94. With such high (nearly unitary) overlap, it is conceivable to take the $|spf\rangle$ as an effective model state for the strongly LL-mixed incompressible phase.

We get a more general view as we extend such numerical comparison in the full investigated parameter space. The result for an example $N_e = 12$ system with a square unit cell is shown in Fig. 4. In the incompressible region, the symmetrized Pfaffian state at each characteristic sector exhibits a larger wave function overlap with the Coulomb ground state than a sole Pfaffian (or anti-Pfaffian) state. It is also notable in Figs. 4(b) and 4(d) that the most distributive zone (with overlaps larger than 0.90 and up to 0.973) of the symmetrized Pfaffian state is consistent with the emerging phase transition region of $\kappa_{\text{eff}} \in [2, 3]$. This reassures our supposition of the incompressible state with large LL mixing as a PH-symmetrized Pfaffian state.

Combining the results from PCA and wave function overlaps, we are able to draw a sketch of a phase diagram with three different phases in the (B, W) parameter space as shown in Fig. 5. The blue region corresponding to the case with a dominant second PC represents a compressible phase. The green region where the sample a locates is an incompressible phase with emergence of the third PC, which can be well described by the PH-symmetrized Pfaffian wave function. The last phase represented in red is another incompressible phase with weaker LL mixing.

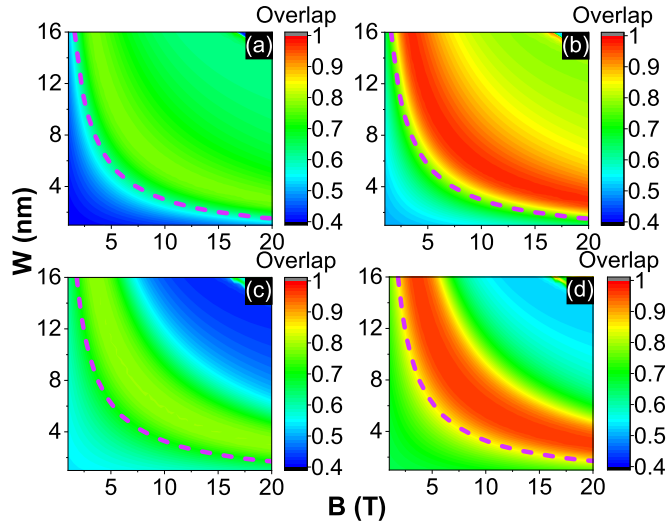

FIG. 4. The wave function overlap between the Coulomb ground state and a candidate model state distributes in the (B, W) parameter space for an $N_e = 12$ system on the torus with a square unit cell. The plots (a) and (b) are at the (0,6) pseudomomentum sector while the plots (c) and (d) are at the (6,6) sector. The candidate state in (a) and (c) is a Pfaffian state while the candidate state in (b) and (d) is the PH-symmetrized Pfaffian state. Dashed curves here mark the compressible-incompressible phase boundaries as in Fig. 2.

Thus far, one important question for the incompressible phase with a large LL mixing is raised: Whether the topology of the Pfaffian state and the anti-Pfaffian state is canceled in such a symmetrized Pfaffian state where the Pfaffian and anti-Pfaffian states have the same weight. If

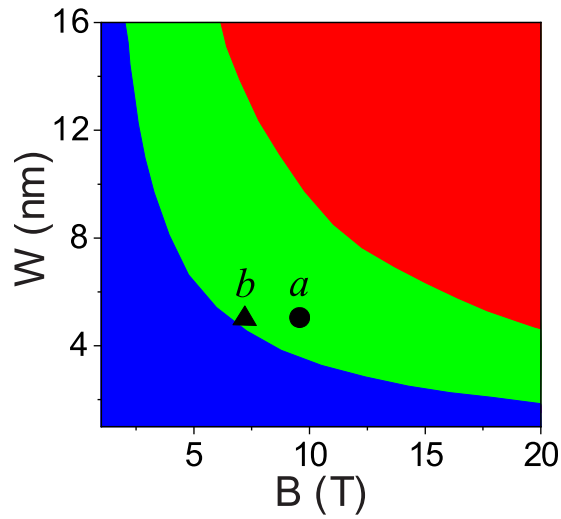

FIG. 5. The sketch of the phase diagram in (B, W) parameter space, obtained according to the ground state at the sector (6,6) of the $N_e = 12$ system given in Fig. 2. The boundary of the compressible phase (blue region) and the incompressible phase (green region) is the same as the dashed line in Figs. 2(c), 2(d), 4(c), and 4(d). The green region is the incompressible phase where the third PC appears and is described by the PH-symmetrized Pfaffian state. The red region is another incompressible phase with the large first PC and weaker LL mixing.

so, the ground state of the $\frac{5}{2}$ FQHE in ZnO, not like the PH-Pfaffian state [9], is then topologically trivial and the non-Abelian excitation disappears. To explore the topological properties of such an incompressible state, which is close to the symmetrized Pfaffian state, we calculate its entanglement spectrum.

C. Entanglement spectrum

The entanglement spectrum is composed of "levels" ξ which are obtained by the singular value decomposition of the matrix form of the ground state and are related to the entanglement entropy [21]. To compute the entanglement spectrum of the ground state, we need to divide the many-body state into two parts, block A and block B. For completeness, we work in both the spherical and toroidal geometries.

In the spherical geometry, based on the previous Hall viscosity calculation, we take the shift $S = 1$ to calculate the screened Coulomb system at the selected parameter set. The obtained spectrum reveals the system is incompressible with a nondegenerate ground state gapped from other higher energy states. In calculating the entanglement spectrum of this incompressible ground state, we set the bipartition block A to mostly locate on the semisphere with a positive z component of the angular momentum. The electron numbers of two partition blocks are $N_{A(B)}$ and it requires that $N_A + N_B = N_e$. The orbit numbers of two blocks are $N_{orb}^{A(B)}$ with $N_{orb}^A + N_{orb}^B = N_s$. The z components of the total angular momenta of two blocks are $L_z^{A(B)}$ with $L_z^A + L_z^B = 0$.

The low-level entanglement spectra of different divisions for an example $N_e = 14$ system are drawn in Figs. 6(a)–6(c). These spectra show a two-sided structure and at the edge of each side there are several lower levels gapped from higher levels. These gapped lower levels exhibit certain patterns, such as 1,1,3,5,... or 1,2,4,7,..., when one counts them along the L_z^A decreasing (increasing) direction at the large (small) L_z^A side. These unique edge-level counting patterns match with the "fingerprint" feature of a Pfaffian or an anti-Pfaffian state according to the conformal field theory (CFT). As a reference, we also draw the entanglement spectra of a Pfaffian state (with $N_e = 16$ and shift $S = 3$) and its PH-conjugate state, the anti-Pfaffian state (with $N_e = 14$ and shift $S = -1$), at different root configuration cutting edges in Figs. 6(d)–6(f) and Figs. 6(g)–6(i), respectively. There, the spectra of the (anti-)Pfaffian exhibit a one-sided gapped edge with the fingerprint patterns counted decreasingly for Pfaffian and increasingly for anti-Pfaffian. Thus, the incompressible Coulomb state owns topological features of both the Pfaffian and the anti-Pfaffian state. However, we could not straightly construct a combination state of a Pfaffian and an anti-Pfaffian on the sphere since these two states have different spherical shifts. Consequently, we could not go further to check the agreement between the screened Coulomb state and the PH-symmetrized Pfaffian state in spherical geometry. The comparison between them can be achieved in the toroidal geometry.

On the torus, the entanglement spectrum of a FQHE state shows a towerlike structure [30], which is quite different from the spherical case since herein each bipartition block contains two chiral edges. In the thin-torus limit, the entire

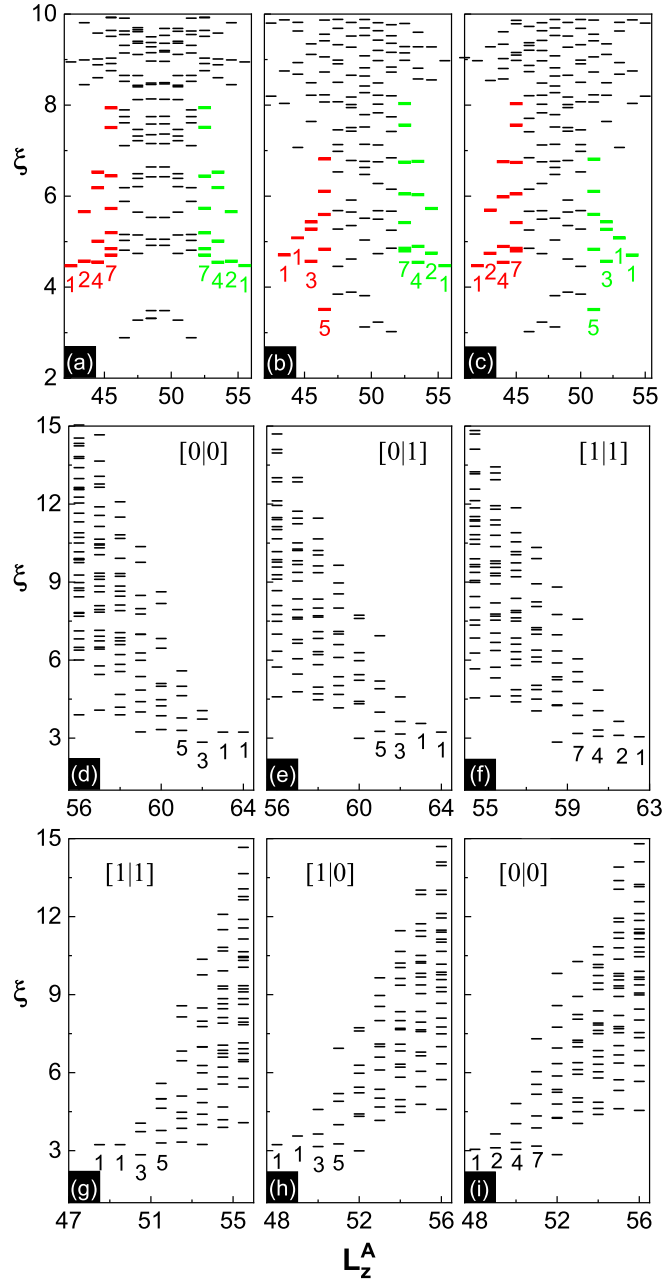

FIG. 6. (a)–(c) Low-level entanglement spectra of the Coulomb ground state for an $N_e = 14$ system on the sphere with the shift $S = 1$ at different bipartition sets of (a) $(N_A, N_{orb}^A) = (N_B, N_{orb}^B) = (7, 14)$, (b) $(N_A, N_{orb}^A) = (6, 13)$, and (c) $(N_A, N_{orb}^A) = (7, 13)$. In comparison, the entanglement spectra of a Pfaffian state with $N_e = 16$ and $S = 3$ are shown in (d)–(f) for different bipartition cuttings based on the root configuration of the Pfaffian state [21]. As the PH-conjugate counterpart, the entanglement spectra of an anti-Pfaffian state with $N_e = 14$ and $S = -1$ are also shown in corresponding panels (g)–(i) for reference. In all cases, the gapped lower levels at spectrum edges exhibit special counting patterns as labeled in the plots.

entanglement spectrum can be understood as a direct supposition of the two nearly independent CFT edges since they are far away from each other. However, as the toroidal geometry deviates from this limit, e.g., with a square unit cell, two CFT edges get more correlated due to a short distance. In

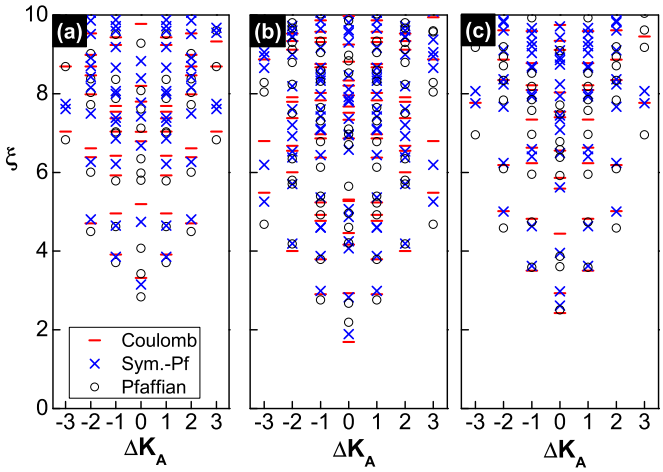

FIG. 7. The entanglement spectra of the Coulomb ground state, Pfaffian state, and PH-symmetrized Pfaffian state at the pseudomomentum sectors (a) (0,6), (b) (6,0), and (c) (6,6) for an $N_e = 12$ system on the torus with a square unit cell. The bipartition blocks are evenly cut with $N_{A(B)} = 6$ and $N_{orb}^{A(B)} = 12$. Only the major tower around $|\Delta K_a| < 4$ is shown for a better comparison.

this case, the spectrum becomes more complex, in lack of a simple physical description. Nevertheless, one can probe the topological property of a FQHE state with the toroidal entanglement spectra by comparing its low-lying levels to those candidate model states.

In Fig. 7, we exhibit the entanglement spectrum of the ground states, Pfaffian state, and PH-symmetrized Pfaffian state at $(N_e/2, 0)$, $(0, N_e/2)$, and $(N_e/2, N_e/2)$ sectors for the $N_e = 12$ system with each block containing $N_e/2$ electrons and $N_s/2$ orbits. Smaller systems provide similar results. At each sector, the spectrum levels are calculated according to the translational momentum K_A, which is a sum (mod N_s) of the orbit indices for all occupied electrons in block A. In addition, we note that the Pfaffian and the anti-Pfaffian states own the same edge environment due to the PH symmetry, thus sharing the identical entanglement spectrum. We focus on the major tower structure around the minimum level of which the momentum is shifted to be $K_A = 0$. It clearly shows that the low-lying levels of the ground-state entanglement spectrum closely match with those of the symmetrized Pfaffian state both in their level positions and their patterns while there is some mismatching with the sole Pfaffian (anti-Pfaffian) state, indicating that the sample a would rather share the same topological universality class with the symmetrized Pfaffian state.

The above analysis reassures that the strongly screened Coulomb state can be well described by a PH-symmetrized Pfaffian state and is confirmed to carry the nontrivial dual topological nature of the Pfaffian and anit-Pfaffian states.

V. SUMMARY

In this paper, we study the strongly LL-mixed $\frac{5}{2}$ fractional quantum Hall system with even number of electrons and a finite width of the quantum well by adapting a screened Coulomb interaction as the effective Hamiltonian. The calculated low-lying spectra reveal a three-fold manifold feature in a certain region of the parameter space made of the magnetic field and quantum well width. With the PCA on the wave functions of these manifold states, we detect a compressible-incompressible phase transition in the parameter space by the competition between the first two leading PCs, which is consistent with the ZnO experiments and early works on an odd-electron system. The significant presence of a subdominant third PC inside the incompressible region suggests an additional transition as the LL mixing grows into a certain strength range, which agrees with the discovery in some early experiments and numerical works with zero-width quantum well. Further calculations on this emerging phase with the Hall viscosity and wave function overlaps show that its ground states own PH symmetry and match well with the PH-symmetrized Pfaffian state rather than a sole PH-nonsymmetric Pfaffian or anti-Pfaffian state. The investigation of the entanglement spectra in both spherical and toroidal geometries demonstrates that this strongly LL-mixed phase carries the nontrivial topological properties with dual features of the Pfaffian and anti-Pfaffian states.

Our results show that the $\frac{5}{2}$ FQHE experimentally observed in the ZnO system has different topological properties from the conventional GaAs system which is believed to be governed by the (anti)Pfaffian state. Such a strongly LL-mixed FQHE state is another favorable plateau to utilize the even denominator FQHE [31], of which non-Abelian excitations are expected. In a thermal transport experiment, two Majorana modes with half-integer Hall thermal conductance are expected. Although the two channels are in opposite directions and may be canceled overall, in a partial equilibrated transport [7] the two different modes may be distinguished to some extent in the ZnO system.

ACKNOWLEDGMENTS

W.L. is supported by the NSF China under Grant No. 11804396. H.W. is supported by the Guangdong Provincial Key Laboratory uncer Grant No. 2019B121203002. We are grateful to the High Performance Computing Center of Central South University for partial support of this work.

[1] K. von Klitzing, T. Chakraborty, P. Kim, V. Madhavan, X. Dai, J. McIver, Y. Tokura, L. Savary, D. Smirnova, A. M. Rey, C. Felser, J. Gooth, and X. Qi, Nat. Rev. Phys. **2**, 397 (2020); J. P. Eisenstein, in *Perspectives in Quantum Hall Effects*, edited by S. Das Sarma and A. Pinczuk (Wiley-Interscience, NewYork, 1996), p. 37; R. L. Willett, Rep. Prog. Phys. **76**, 076501 (2013); X. Lin, R. Du, and X. Xie, Nat. Sci. Rev. **1**, 564 (2014); A. A. Zibrov, E. M. Spanton, H. Zhou, C. Kometter, T. Taniguchi, K. Watanabe, and A. F. Young, Nat. Phys. **14**, 930 (2018); Y. Kim, A. C. Balram, T. Taniguchi, K. Watanabe, J. K. Jain, and J. H. Smet, *ibid.* **15**, 154 (2019).

[2] B. I. Halperin, Helv. Phys. Acta **56**, 75 (1983).

[3] G. Moore and N. Read, Nucl. Phys. B **360**, 362 (1991); N. Read and D. Green, Phys. Rev. B **61**, 10267 (2000); N. Read, Phys. B: Condens. Matter **298**, 121 (2001).

[4] M. Levin, B. I. Halperin, and B. Rosenow, Phys. Rev. Lett. **99**, 236806 (2007); S.-S. Lee, S. Ryu, C. Nayak, and M. P. A. Fisher, *ibid.* **99**, 236807 (2007); H. Wang, D. N. Sheng, and F. D. M. Haldane, Phys. Rev. B **80**, 241311(R) (2009).

[5] M. Banerjee, M. Heiblum, V. Umansky, D. E. Feldman, Y. Oreg, and A. Stern, Nature (London) **559**, 205 (2018).

[6] D. F. Mross, Y. Oreg, A. Stern, G. Margalit, and M. Heiblum, Phys. Rev. Lett. **121**, 026801 (2018); C. Wang, A. Vishwanath, and B. I. Halperin, Phys. Rev. B **98**, 045112 (2018); B. Lian and J. Wang, *ibid.* **97**, 165124 (2018); P.-S. Hsin, Y.-H. Lin, N. M. Paquette, and J. Wang, Phys. Rev. Res. **2**, 043242 (2020).

[7] S. H. Simon and B. Rosenow, Phys. Rev. Lett. **124**, 126801 (2020).

[8] M. Greiter, X.-G. Wen, and F. Wilczek, Phys. Rev. Lett. **66**, 3205 (1991); N. Read and E. Rezayi, Phys. Rev. B **59**, 8084 (1999); K. K. W. Ma and D. E. Feldman, *ibid.* **100**, 035302 (2019).

[9] D. T. Son, Phys. Rev. X **5**, 031027 (2015).

[10] W. Bishara and C. Nayak, Phys. Rev. B **80**, 121302(R) (2009); E. H. Rezayi and F. D. M. Haldane, *ibid.* **42**, 4532 (1990); E. H. Rezayi and S. H. Simon, Phys. Rev. Lett. **106**, 116801 (2011); I. Sodemann and A. H. MacDonald, Phys. Rev. B **87**, 245425 (2013); R. E. Wooten, J. H. Macek, and J. J. Quinn, *ibid.* **88**, 155421 (2013); M. R. Peterson and C. Nayak, *ibid.* **87**, 245129 (2013); Phys. Rev. Lett. **113**, 086401 (2014); E. H. Rezayi, *ibid.* **119**, 026801 (2017).

[11] J. Falson, D. Maryenko, B. Friess, D. Zhang, Y. Kozuka, A. Tsukazaki, J. H. Smet, and M. Kawasaki, Nat. Phys. **11**, 347 (2015).

[12] J. Falson, D. Tabrea, D. Zhang, I. Sodemann, Y. Kozuka, A. Tsukazaki, M. Kawasaki, K. von Klitzing, and J. H. Smet, Sci. Adv. **4**, eaat8742 (2018).

[13] J. Falson, Phys. E **110**, 49 (2019); J. Falson and M. Kawasaki, Rep. Prog. Phys. **81**, 056501 (2018).

[14] J. Yang, S. Tran, J. Wu, S. Che, P. Stepanov, T. Taniguchi, K. Watanabe, H. Baek, D. Smirnov, R. Chen, and C. Ning Lau, Nano Lett. **18**, 229 (2018).

[15] P. T. Zucker and D. E. Feldman, Phys. Rev. Lett. **117**, 096802 (2016); S. Das, S. Das, and S. S. Mandal, arXiv:2206.04419; L. Herviou and F. Mila, arXiv:2210.04925.

[16] I. L. Aleiner and L. I. Glazman, Phys. Rev. B **52**, 11296 (1995); M. M. Fogler, in *High Magnetic Fields: Applications in Condensed Matter Physics and Spectroscopy*, edited by C. Berthier, L.-P. Levy, and G. Martinez (Springer-Verlag, Berlin, 2002); W. Luo and R. Côté, Phys. Rev. B **90**, 245410 (2014).

[17] W. Luo and T. Chakraborty, Phys. Rev. B **93**, 161103(R) (2016); **94**, 161101(R) (2016).

[18] W. Luo and T. Chakraborty, Phys. Rev. B **96**, 081108(R) (2017).

[19] W. Luo, S. Peng, H. Wang, Y. Zhou, and T. Chakraborty, Phys. Rev. B **104**, L161302 (2021).

[20] N. Jiang, S. Ke, H. Ji, H. Wang, Z.-X. Hu, and X. Wan, Phys. Rev. B **102**, 115140 (2020); N. Jiang and M. Lu, Chin. Phys. Lett. **37**, 117302 (2020); Q. Jin and H. Wang, Phys. Lett. A **427**, 127921 (2022); Phys. B: Condens. Matter **629**, 413635 (2022).

[21] H. Li and F. D. M. Haldane, Phys. Rev. Lett. **101**, 010504 (2008).

[22] F. D. M. Haldane, Phys. Rev. Lett. **55**, 2095 (1985).

[23] T. Chakraborty and P. Pietiläinen, *The Quantum Hall Effects* (Springer, New York, 1995); *The Fractional Quantum Hall Effect* (Springer, New York, 1988).

[24] M. R. Peterson, Th. Jolicoeur, and S. Das Sarma, Phys. Rev. Lett. **101**, 016807 (2008).

[25] N. Samkharadze, D. Ro, L. N. Pfeiffer, K. W. West, and G. A. Csáthy, Phys. Rev. B **96**, 085105 (2017).

[26] N. Read, Phys. Rev. B **79**, 045308 (2009); N. Read and E. H. Rezayi, *ibid.* **84**, 085316 (2011).

[27] X. G. Wen and A. Zee, Phys. Rev. Lett. **69**, 953 (1992).

[28] E. H. Rezayi and F. D. M. Haldane, Phys. Rev. Lett. **84**, 4685 (2000).

[29] W. Zhu, D. N. Sheng, and K. Yang, Phys. Rev. Lett. **125**, 146802 (2020).

[30] A. M. Läuchli, E. J. Bergholtz, and M. Haque, New J. Phys. **12**, 075004 (2010); Z. Liu, E. J. Bergholtz, H. Fan, and A. M. Läuchli, Phys. Rev. B **85**, 045119 (2012).

[31] C. Nayak, S. H. Simon, A. Stern, M. Freedman, and S. Das Sarma, Rev. Mod. Phys. **80**, 1083 (2008); X. Wan, Z. Wang, and K. Yang, Physics (Beijing) **42**, 558 (2013).